

## Structured water in polyelectrolyte dendrimers: Understanding small angle neutron scattering results through atomistic simulation

Bin Wu, Bouthaina Kerkeni, Takeshi Egami, Changwoo Do, Yun Liu et al.

Citation: *J. Chem. Phys.* **136**, 144901 (2012); doi: 10.1063/1.3697479

View online: <http://dx.doi.org/10.1063/1.3697479>

View Table of Contents: <http://jcp.aip.org/resource/1/JCPSA6/v136/i14>

Published by the [American Institute of Physics](#).

---

### Additional information on J. Chem. Phys.


Journal Homepage: <http://jcp.aip.org/>

Journal Information: [http://jcp.aip.org/about/about\\_the\\_journal](http://jcp.aip.org/about/about_the_journal)

Top downloads: [http://jcp.aip.org/features/most\\_downloaded](http://jcp.aip.org/features/most_downloaded)

Information for Authors: <http://jcp.aip.org/authors>

## ADVERTISEMENT



**Special Topic Section:**  
**PHYSICS OF CANCER**

Why cancer? Why physics? [View Articles Now](#)

# Structured water in polyelectrolyte dendrimers: Understanding small angle neutron scattering results through atomistic simulation

Bin Wu,<sup>1,2,3</sup> Boutheïna Kerkeni,<sup>4</sup> Takeshi Egami,<sup>5,6</sup> Changwoo Do,<sup>1</sup> Yun Liu,<sup>7,8</sup>  
Yongmei Wang,<sup>9</sup> Lionel Porcar,<sup>10</sup> Kunlun Hong,<sup>2</sup> Sean C. Smith,<sup>2</sup> Emily L. Liu,<sup>3</sup>  
Gregory S. Smith,<sup>1</sup> and Wei-Ren Chen<sup>1,a)</sup>

<sup>1</sup>Biology and Soft Matter Division, Oak Ridge National Laboratory, Oak Ridge, Tennessee 37831, USA

<sup>2</sup>Center for Nanophase Materials Sciences, Oak Ridge National Laboratory, Oak Ridge, Tennessee 37831, USA

<sup>3</sup>Department of Mechanical, Aerospace and Nuclear Engineering, Rensselaer Polytechnic Institute, Troy, New York 12180, USA

<sup>4</sup>Unité de Physico-Chimie Moléculaire, IPEST, Université de Carthage, La Marsa, Tunis, Tunisia

<sup>5</sup>Department of Materials Science and Engineering and Department of Physics and Astronomy, The University of Tennessee, Knoxville, Tennessee 37996-1508, USA

<sup>6</sup>Department of Physics and Astronomy, The University of Tennessee, Knoxville, Tennessee 37996-1200, USA

<sup>7</sup>Department of Chemical Engineering, University of Delaware, Newark, Delaware 19716, USA

<sup>8</sup>The NIST Center for Neutron Research, National Institute of Standards and Technology, Gaithersburg, Maryland 20899-6100, USA

<sup>9</sup>Department of Chemistry, the University of Memphis, Memphis, Tennessee 38152-3550, USA

<sup>10</sup>Institut Laue-Langevin, B.P. 156, F-38042 Grenoble CEDEX 9, France

(Received 19 December 2011; accepted 5 March 2012; published online 11 April 2012)

Based on atomistic molecular dynamics (MD) simulations, the small angle neutron scattering (SANS) intensity behavior of a single generation-4 polyelectrolyte polyamidoamine starburst dendrimer is investigated at different levels of molecular protonation. The SANS form factor,  $P(Q)$ , and Debye autocorrelation function,  $\gamma(r)$ , are calculated from the equilibrium MD trajectory based on a mathematical approach proposed in this work. The consistency found in comparison against previously published experimental findings (W.-R. Chen, L. Porcar, Y. Liu, P. D. Butler, and L. J. Magid, *Macromolecules* **40**, 5887 (2007)) leads to a link between the neutron scattering experiment and MD computation, and fresh perspectives. The simulations enable scattering calculations of not only the hydrocarbons but also the contribution from the scattering length density fluctuations caused by structured, confined water within the dendrimer. Based on our computational results, we explore the validity of using radius of gyration  $R_G$  for microstructure characterization of a polyelectrolyte dendrimer from the scattering perspective. © 2012 American Institute of Physics. [<http://dx.doi.org/10.1063/1.3697479>]

## I. INTRODUCTION

Polyelectrolyte dendrimers are regularly branched synthetic macromolecules who bear ionizable constituent components.<sup>1,2</sup> With suitable structural modifications, they have been proposed for delivery applications such as guest material carries.<sup>3,4</sup> Since the seminal work by Muthukumar and Welch,<sup>5</sup> extensive effort of computer simulation has been devoted to the structural study of polyelectrolytes for some 15 years.<sup>6–26</sup> One major subject of polyelectrolyte dendrimer computational structural investigations has been addressing the response of single dendrimer to molecular charge. Typically, either the variation of dendrimer global size, in terms of radius of gyration  $R_G$ , or the evolution of intra-dendrimer density profile along the radial direction is calculated. It is particularly useful to test these structural predictions against the corresponding physical quantities obtained experimentally. It is only recently that the conformational dependence

on molecular charge has become the primary focus of a series of small angle neutron scattering (SANS) experimental investigations.<sup>30–38</sup> Small angle scattering experiments complement the simulations, due to their accessibility to the relevant mesoscopic length scales ranging from several Å to some hundreds nanometers.<sup>27–29</sup> Consistent with most of the computational predictions, the intra-dendrimer density profiles extracted from SANS data analysis suggest that the dense-core profile is indeed a generic feature polyelectrolyte polyamidoamine (PAMAM) dendrimers, regardless of the dendrimer molecular weight. Upon increasing the molecular protonation, a significant variation in  $\rho(r)$ , the density profile of the polymer, from a dense-core profile to a more uniformly distributed one, has been observed, suggesting the evolution of several generations of PAMAM dendrimer from low generation ones with open architecture to high generation ones with more tightly packed molecular structure. The observed charge-triggered electrostatic swelling along with a moderate increase in  $R_G$  was not predicted in earlier simulation studies of polyelectrolyte dendrimers, but it is in fair agreement with that from later atomistic molecular dynamics (MD) calculations.<sup>16,24</sup> A recent contrast variation SANS

<sup>a)</sup> Author to whom correspondence should be addressed. Electronic mail: chenw@ornl.gov.

experiment indicated this charge-triggered conformational variation is accompanied by an increase in the intra-molecular hydration level. Quasi-elastic neutron scattering (QENS) further revealed the enhancement of local segmental dynamics upon increasing the molecular protonation of dendrimer. However, this dynamical observation is intrinsically different from the progressively sluggish picture predicted by Brownian dynamics simulation.<sup>39</sup> The bi-directional information flow and mutual guidance between MD investigation and scattering experiment, via scrutinizing the aforementioned structural and dynamical characteristics, indeed provides a broader grasp of fundamental understanding of the microscopic mechanisms underlying the pH-responsive behaviors in this very important class of material.

Evidenced by the documented research activities, constructing a better model for PAMAM dendrimers remain as an active research subject for computational study. Atomistic MD work conducted by Goddard and coworkers<sup>16</sup> focused on improving simulation models based on existing experimental structural characteristics. With the Dreiding III force field whose intermolecular parameters were optimized quantum mechanically, their predicted numerical values of radius of gyration ( $R_G$ ) of G4 PAMAM dendrimer showed excellent agreement with earlier SANS model fitting results<sup>30</sup> within experimental uncertainties at three different levels of molecular protonation. A similar quantitative success for G4, G5, and G7 PAMAM dendrimers is also found in a recent simulation work by Lee and Larson.<sup>24</sup> These models were able to improve the agreement with  $R_G$  from SANS measurements of the PAMAM dendrimer.

In this paper, we challenge the conventional idea that  $R_G$  provides the best measure of the global size of an object regarding its geometric shape, and question whether it can be applied to a wider class of structural features. It is not the intention of this work to keep pursuing the quantitative accuracy of simulation via the approach of force field modification. Instead, we attempt to provide an alternative perspective, via computing more fundamental spatial correlation functions rather than scalar parameters such as  $R_G$  which only contain contracted structural information, demonstrating other existing possibilities in which better agreement between MD and neutron scattering experiments can also be achieved. As a demonstration, we develop a rigorous methodology to calculate the spatial correlation functions from equilibrium MD trajectories and explore the effect of confined water structuring on the scattering signature of single PAMAM dendrimer. While a significant difference is revealed in the scattering functions calculated from the same trajectory with and without the incorporation of confined water effect,  $R_G$  shows little susceptibility to this variation in computing algorithm. This suggests that a MD model, which renders better quantitative agreement in  $R_G$  with experiment, does not necessarily guarantee a more accurate description of the microstructure without establishing proper comparability with experiment in trajectory analysis.

This paper is organized as follows: Sec. II gives a brief discussion about simulation procedures. Results of our equilibrium MD trajectory analysis are given in Sec. III. We summarize this report in Sec IV.

## II. ATOMISTIC MOLECULAR DYNAMICS SIMULATION

The AMBER molecular dynamics package,<sup>40</sup> commonly used to evaluate the structural characteristics of various dendrimers,<sup>8,9,41–43</sup> was employed in this study to investigate the small angle scattering behavior of a generation 4 (G4) PAMAM dendrimer and its dependence on molecular charge under the explicit solvent conditions. Within the Amber framework, the procedure of constructing G4 PAMAM dendrimer is briefly described as follows: Three different residues, representing the core, repeating, and ending blocks, respectively, were first created as the fundamental building elements. The core residue consists of an ethylenediamine (EDA) molecule and two amine groups, each of which provides the connection to two repeating residues. The amidoamine present in each repeating unit is further connected with two other repeating units, which are characterized as the next generation. The simulation model of a single PAMAM dendrimer can be constructed iteratively based on the generation with the connecting point of the molecular peripheral unit of hydrogen. Different sets of residues with different levels of amino protonation were used in different G4 PAMAM dendrimer models to represent different pH conditions. The atomic partial charges were derived using the AM1/BCC method, and general amber force field (GAFF; Refs. 44–47) is employed to account for inter-atomic interactions, both of which are available in the AmberTools package of the AMBER11 software.<sup>46</sup>

First, energy minimization was applied to the input structure to exclude an unrealistically excessive interaction energy resulting from abnormal distances between neighboring atoms. This was followed by simulated annealing for the sake of accelerating the simulation. Chloride ions were introduced to maintain the overall charge neutrality for the case of charged dendrimer with positively charged amines. TIP3P (Ref. 47) water was used to solvate the system into a truncated octahedral simulation box to ensure there are at least 8 Å between the outmost molecular periphery of dendrimer along any radial direction and the boundary of the simulation box.

After the aforementioned preparation process, the simulation was brought to equilibrium under following conditions. Temperature and pressure were maintained at 300 K and 1 bar through applying Langevin dynamics<sup>48</sup> and *NPT* ensemble. The cutoff distance for force evaluation was chosen to be 10 Å. Particle-mesh Ewald summation<sup>49</sup> and periodic boundary condition were employed. All bonds involving hydrogen atoms were applied with SHAKE constraints.<sup>50</sup> Each simulation case was run at least 7 ns and the trajectories for the last 2 ns were used for the structural analysis presented in Sec. III. The simulation was carried out using the Oak Ridge Institutional cluster available at Spallation Neutron Source, Oak Ridge National Laboratory.

## III. RESULTS AND DISCUSSION

In neutron scattering experiments on colloids, the equilibrium structure of the targeted system is generally approximated as a two-phase system: the suspending colloidal particles and the continuous liquid phase consisting of solvent

molecules.<sup>51,52</sup> Due to the large asymmetry in size between the particles and solvent molecules, the solvent is generally considered as a structureless continuum on the characteristic length scale of the particles. From the perspective of scattering SANS experiment, scattering (except at zero-angle) is the consequence of the compositional and density differences between the particles and solvent. A less conceivable contribution is from the density fluctuation caused by the restructuring of solvent around the vicinity of colloid. Although the chemical composition of the solvent (and therefore the bound scattering length) remains invariant, the difference in the spatial packing of solvent around the colloidal surface and the unperturbed bulk state can indeed generate sufficient change in the scattering length density (SLD),  $\rho(r)$ , due to density fluctuation and hence affect the scattering behavior perceptibly.

Effects of water structure on the structural and dynamical characteristics of various soft matter systems have been observed.<sup>53,54</sup> For example, based on osmotic stress force measurements, the correlation of the attractive interaction between DNA strands which cannot be explained by classical Derjaguin-Landau-Verwey-Overbeek (DLVO) theory,<sup>55</sup> and restructuring of surficial water between neighboring double helices is indicated by Rau and Parsegian.<sup>55-57</sup> Using static and dynamic light scattering measurements, Petsev and Vekilov<sup>58</sup> also attribute the origin of their observed anomalous non-DLVO hydration interactions between apoferritin proteins to the interfacial water structuring. Moreover, the microscopic structure of a water layer on the surface of colloidal silica is further revealed by Shibayama and coworkers<sup>59</sup> using contrast variation SANS. Deduced from the dynamics of confined water molecules, hierarchical water structure near the surface of nanopowder rutile (TiO<sub>2</sub>) and cassiterite (SnO<sub>2</sub>) is found by Mamontov and coworkers<sup>60</sup> using QENS technique complemented by MD simulation.

The pair distribution function<sup>61,62</sup> has been extensively used when the structure of water is studied. In this study, the intra-molecular and interfacial water structure around neutral and charged G4 PAMAM dendrimers can be visualized from the intermolecular oxygen-oxygen partial pair correlation functions defined as follows:

$$g_{O_I O}(r) = \left\langle \sum_{i \in O_I} \sum_{j \in O, j \neq i} \frac{1}{4\pi|r_{ij}|} \delta(r - |r_{ij}|) \right\rangle_{O_I}, \quad (1)$$

where  $r_{ij}$  is the distance between  $i$ th and  $j$ th oxygen. The water molecules contained in the simulation box are categorized according to their distance to the nearest constituent atom of the polymeric components of dendrimer. In Eq. (1),  $O_I$  represents the subset of water molecules among all water molecules  $O$  with an oxygen atom residing within the specified distance away from dendrimer surface, and  $\langle \rangle$  represents the necessary subset, angular, and frame averaging processes. The normalized partial pair correlation functions  $g_{oo}(r)$  are given in Figure 1 for various charge states (neutral ( $\alpha = 0$  according to our previous notation), primary amines protonated ( $\alpha = 1$ ), and fully protonated ( $\alpha = 2$ )). As the distance from the dendrimer increases, the height of the first peak of  $g_{oo}(r)$ , which contains the information of local ordering, increases steadily until the layer distance reaches 4 Å. This observation indicates that the packing of water molecules whose distance to the dendrimer is less than 4 Å is characteristically different from that of bulk water molecules. This evolution of  $g_{oo}(r)$  represents the existence of surficial water restructuring. An interfacial water layer with thickness of 4 Å, within which the packing density of water is seen to decrease progressively towards the dendrimer periphery, is indicated by our MD model at all three different levels of molecular protonation. Therefore, in addition to the polymeric components of dendrimer and counterions (Figure 2(a)), these confined water molecules with packing different from that of bulk water (Figure 2(b)) will give rise to scattering, and one must calculate the coherent scattering cross section from simulation results. To ensure direct comparability between MD and experiment, another critical issue needs to be addressed: In the equilibrium MD trajectory, each atom is represented by a Dirac delta function weighted by the corresponding bound scattering length. To properly reflect the scattering probability of a neutron from each spatial position, a certain volume is required to assign to each atom so that the local SLD  $\rho(r)$  can be obtained from the bound scattering length of each corresponding atom. Typically, one approximates each constituent atom as a hard sphere with a finite size van der Waals (VDW) radius and models the simulated system as an assembly of spheres. From the equilibrium trajectory, the corresponding Debye correlation function  $\gamma(r)$  (Ref. 64) can be calculated using the dumbbell model proposed by Glatter.<sup>65</sup> The scattering intensity can therefore be generated from  $\gamma(r)$  via Fourier transform once the excessive local SLD  $\Delta\rho(r)$  for each constituent hard sphere is

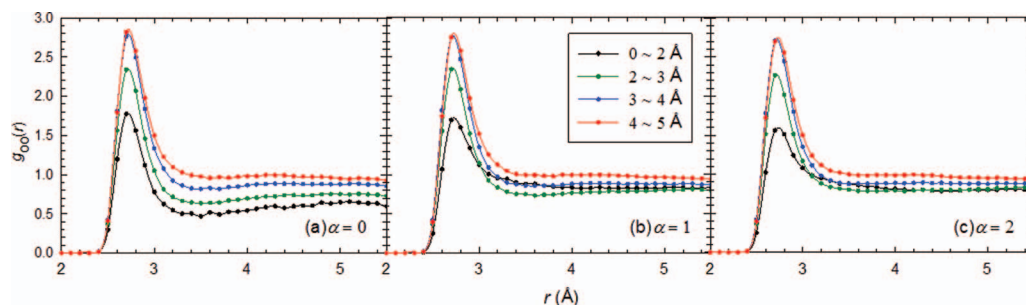


FIG. 1. The pair distribution function of oxygen-oxygen distance  $g_{oo}(r)$  for TIP3P water around the vicinity of a G4 PAMAM dendrimer of different molecular protonation level: (a) neutral ( $\alpha = 0$ ), (b) protonated primary amines ( $\alpha = 1$ ), and (c) protonated primary and tertiary amines ( $\alpha = 2$ ). It is important to point out that all the reported  $g_{oo}(r)$  reach the asymptotic value of 1 when  $r > 15$  Å.



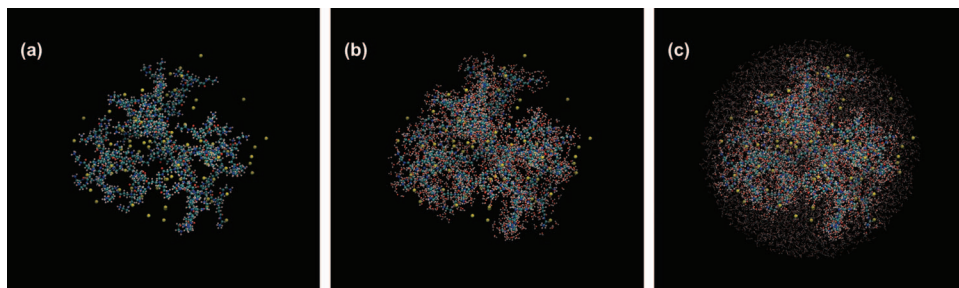


FIG. 2. The snapshot of G4 PAMAM dendrimer of  $\alpha = 2$  created using visual molecular dynamics.<sup>40,63</sup> Selectively chosen atoms from simulation system are shown. Panel (a) illustrates polymeric part of dendrimer as well as counterions. The light blue, white, blue, red, and yellow spheres represent carbon, hydrogen, nitrogen, oxygen, and chloride atoms, respectively. In addition to the atoms present in panel (a), panel (b) incorporates interfacial water which should be recognized as part of the scatterer. The virtual sphere used for calculation of  $P(Q)$  are shown in panel (c).

properly considered. However, this approach is unable to address the scattering contribution from the intra-dendrimer cavities, such as several dark regions presenting in the molecular interior of dendrimer where water cannot penetrate as shown in Figure 2(b). Apparently the scattering contribution of these time-evolving, inaccessible voids is due to the contrast between bulk water and vacuum. However, at any given instance, no atom presents in these unoccupied spatial regions and therefore it is difficult to generally quantify the volume of vacuum without reference points provided by the spatial coordinates of atoms.

To bypass this intrinsic difficulty embedded in this discrete nature of the MD trajectory, a different approach, schematically demonstrated in Figure 2(c), is developed to address the influence of the aforementioned structural issues on the scattering behavior of PAMAM dendrimer. Instead of specifying a local volume of each atom with its VDW radius, a global sphere centered at the geometrical center of dendrimer with sufficiently large radius is assigned to thoroughly incorporate all the polymeric components of dendrimer, intra-dendrimer interfacial water molecules, and voids. The remaining space in the simulation box beyond the spherical boundary is mainly water molecules at the bulk phase under the simulated thermodynamic conditions. By comparing and contrasting the scattering power of the global sphere containing the scatterers and a virtual sphere with same radius but consisting of bulk water molecules only, the scattering behavior of a PAMAM dendrimer, which is a collective manifestation compositional and density fluctuations in comparison to bulk water, can now be rigorously characterized.

To compare with our previous experimental result,<sup>30</sup> the intra-dendrimer structure factor of dendrimer  $P(Q)$ , also known as the form factor, is calculated with three different levels of molecular charge: neutral ( $\alpha = 0$ ), with protonated primary amines ( $\alpha = 1$ ), and fully protonated ( $\alpha = 2$ ). The scattering amplitude, resulting from the contrast between the scatterer and bulk water with uniform density, is given by the following expression:

$$\begin{aligned} F(\vec{Q}) &= F_{MD,sphere}(\vec{Q}) - F_{D_2O,sphere}(\vec{Q}) \\ &= \int_{sphere} \rho_{MD}(\vec{r}) e^{-i\vec{Q}\cdot\vec{r}} d\vec{r} \\ &\quad - \int_{sphere} \rho_{D_2O}(\vec{r}) e^{-i\vec{Q}\cdot\vec{r}} d\vec{r}, \end{aligned} \quad (2)$$

where  $\rho_{MD}(\vec{r}) = \sum_{i=1}^N b(\vec{r}_i) \delta(\vec{r} - \vec{r}_i)$  represent all the  $N$  atoms enclosed in the global sphere. The first term of the right-hand side (RHS) of Eq. (2) therefore can be expressed as

$$\begin{aligned} F_{MD,sphere}(\vec{Q}) &= \int_{sphere} \sum_{i=1}^N b(\vec{r}_i) \delta(\vec{r} - \vec{r}_i) e^{-i\vec{Q}\cdot\vec{r}} d\vec{r} \\ &= \sum_{i=1}^N b(\vec{r}_i) e^{-i\vec{Q}\cdot\vec{r}_i}. \end{aligned} \quad (3)$$

Since  $\rho_{D_2O}(\vec{r}) = \rho_{D_2O}$ , the second term on the RHS of Eq. (2) can be further scalarized as

$$\begin{aligned} F_{D_2O,sphere}(\vec{Q}) &= F_{D_2O,sphere}(Q) \\ &= \rho_{D_2O} \int_{sphere} e^{-i\vec{Q}\cdot\vec{r}} d\vec{r} \\ &= 4\pi\rho_{D_2O} \frac{\sin(QR) - QR \cos(QR)}{Q^3}. \end{aligned} \quad (4)$$

From Eqs. (2)–(4),  $P(\vec{Q})$  can be shown to take the following expression:

$$\begin{aligned} P(\vec{Q}) &= F(\vec{Q})F(\vec{Q})^* \\ &= \left| \sum_{i=1}^N b(\vec{r}_i) e^{-i\vec{Q}\cdot\vec{r}_i} \right|^2 - 2F_{D_2O,sphere}(Q) \\ &\quad \times \left[ \sum_{i=1}^N b(\vec{r}_i) \cos(\vec{Q} \cdot \vec{r}_i) \right] + F_{D_2O,sphere}(Q)^2. \end{aligned} \quad (5)$$

The final form of  $P(Q)$  is obtained after angular and time averaging processes

$$\begin{aligned} P(Q) &= \langle P(\vec{Q}) \rangle \\ &= \left\langle \left| \sum_{i=1}^N b(\vec{r}_i) e^{-i\vec{Q}\cdot\vec{r}_i} \right|^2 \right\rangle - 2F_{D_2O,sphere}(Q) \\ &\quad \times \left\langle \sum_{i=1}^N b(\vec{r}_i) \cos(\vec{Q} \cdot \vec{r}_i) \right\rangle + F_{D_2O,sphere}(Q)^2. \end{aligned} \quad (6)$$

The calculated  $P(Q)$ , along with that generated from SANS model fitting parameters, are presented in Figure 3. As shown

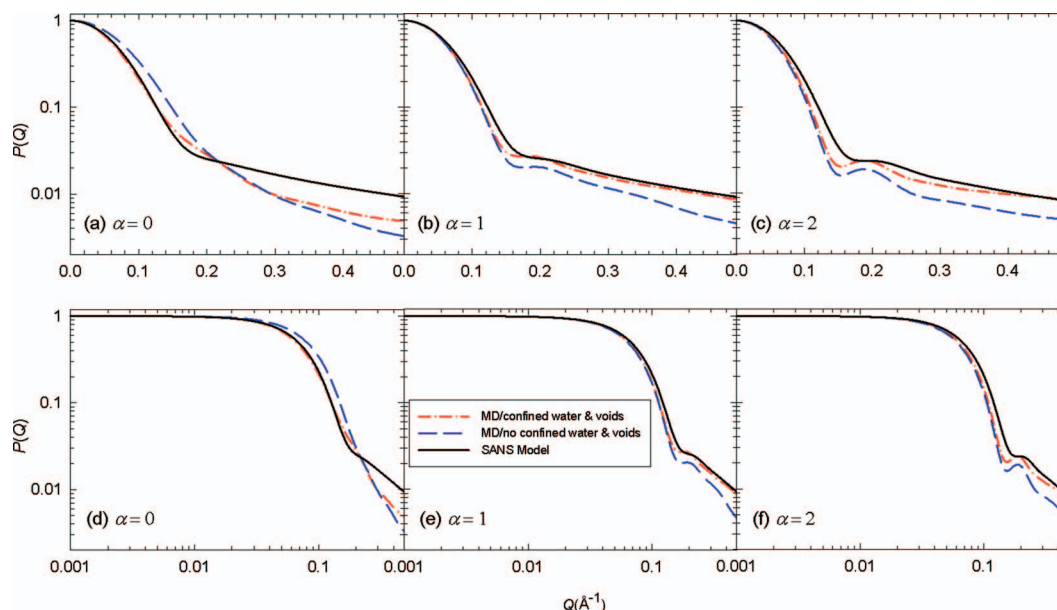


FIG. 3. Comparison of the form factor  $P(Q)$  of G4 PAMAM dendrimer obtained from MD simulation and SANS model fitting as a function of molecular protonation in semi-log plots (Figures 3(a)–3(c)) and logarithmic plots (Figures 3(d)–3(f)). A better quantitative agreement is reached with the incorporation of the scattering contributions from the density fluctuations introduced by confined water structuring and voids.

in the semi-log plots presented in Figures 3(a)–3(c), the calculated  $P(Q)$  which incorporates the additional scattering contribution from the density fluctuations introduced by confined water structuring and intra-molecular voids (red curves) indeed show a better qualitative agreement, especially in the higher- $Q$  region, with experimental  $P(Q)$  (black curves) than the  $P(Q)$  calculated only from the compositional difference between the polymer components of dendrimer and bulk water. The same curves are presented again in Figures 3(d)–3(f) on a logarithm scale. Upon increasing the molecular protonation, our calculated  $P(Q)$  indeed exhibits a gradually enhancing bump centering around  $Q = 0.2 \text{ \AA}^{-1}$  which is consistent with our previous experimental observation.<sup>27</sup> The radius of gyration  $R_G$  has been commonly used in many computational studies of PAMAM dendrimers as an index parameter to describe its size variation in response to external conditions. It is therefore worth exploring its usefulness in characterizing the varying microscopic structure revealed by  $P(Q)$ . It is important to point out that the  $R_G$  deduced from a SANS experiment takes the following expression:

$$R_G^2 = \frac{\int \vec{r}^2 \Delta\rho(\vec{r}) d\vec{r}}{\int \Delta\rho(\vec{r}) d\vec{r}}. \quad (7)$$

Instead of computing  $R_G$  by local SLD  $\rho(\vec{r})$ ,<sup>16</sup> a proper evaluation of  $R_G$  from equilibrium MD trajectories should be made based on the excessive SLD  $\Delta\rho(\vec{r})$  for the sake of direct comparison with SANS experimental results. Upon increasing the molecular protonation from  $\alpha = 0$  to  $\alpha = 2$ , similar to the previous studies, an increase in  $R_G$  from 19 Å to 23 Å is found in our simulation. It is important to point out that, judging from the quantitative values of the  $P(Q)$  calculated from two different methods within the Guinier region<sup>66</sup> ( $QR_G \ll 1$ ), no significant change in  $R_G$  is found when the influence of confined water and intra-molecular voids is incorporated in our computation. It is evident that the detailed

local structural information, which is reflected in the high- $Q$  region of  $P(Q)$ , is lost by the integration process presented in Eq. (7). Therefore, this insensitivity suggests that  $R_G$  can only provide the quantitative information about the global size of a dendrimer and cannot describe more detailed variations in the internal structure of dendrimer-water complex.

An intriguing question about what is the reason for the disagreement between experimental  $P(Q)$  (black curves) and that generated by MD (red curves), even with sophisticated computational methodology and thorough structural consideration, has not been answered unambiguously. It is our conjectures that, inspired by the work of Goddard and coworkers,<sup>16</sup> there might be some room for optimizing the potential parameters of GAFF for atomistic simulation of a polyelectrolyte dendrimer and the improvement might lead to better agreement in comparison with experiment. Minor quantitative differences in  $P(Q)$  are also expected if a different computational water model with different approximation of molecular mechanism is used in the simulation. From the experimental perspective, the approximation of factorizing SANS intensity into intra-molecular form factor  $P(Q)$  and inter-molecular structure factor  $S(Q)$ ,<sup>27</sup> which is valid for monodisperse population of spherical scatterers, used in our SANS data analysis for the sake of its mathematical convenience, may not be able to fully describe the additional correlation between the dendrimer orientations and their spatial positions since the shape of dendrimer is not entirely spherically symmetric especially in its neutral state. This approximation may account for, to some certain extent, the disagreement of  $P(Q)$  in the high- $Q$  region. Moreover, we believe the observed larger disagreement between experimental  $P(Q)$  and that generated by MD for the case of  $\alpha = 0$  is due to the approximation of microscopic properties of water by TIP3P model, whose applicability and limitation has been previously explored.<sup>67</sup> It is possible that various intra-molecular interaction involving

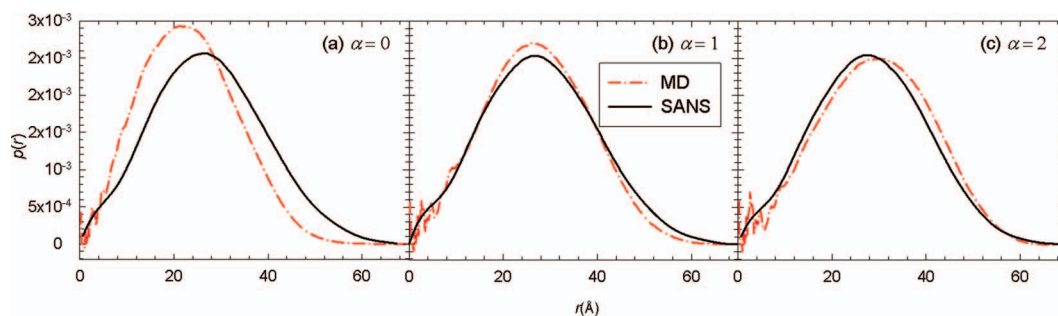


FIG. 4. Comparison of the pair distance distribution function (PDDF)  $p(r)$  of G4 PAMAM dendrimer obtained from MD simulation (red curves) and indirect Fourier transform (IFT) of experimental model fitting data (black curves) at different molecular protonation levels.

invasive water molecules may not be fully addressed quantitatively in the neutral case. For both charged cases, the dendrimer structure is mainly determined by the additional intra-molecular electrostatic interactions, which appears to be better accounted for in the computational model. Consequently, a better quantitative agreement between experiment and MD is seen in Figures 3(b), 3(c), 3(e), and 3(f).

It is instructive to digress briefly into the concept of the aforementioned Debye correlation function  $\gamma(r)$ ,<sup>64</sup> whose usefulness may be demonstrated by comparison with the partition function of equilibrium statistical mechanics. As is well known, all of the thermodynamic properties of any particular system can be obtained by calculating the partition function of a suitable statistical ensemble.<sup>68</sup>  $\gamma(r)$  plays a similar role in determining the material structure from the physical process of elastic scattering: The experimentally measured coherent scattering cross section can be directly linked to  $\gamma(r)$  via a Fourier transform.<sup>28,29</sup> Several diagrammatic representations of small angle scattering data analysis, such as Holtzer plots, Kratky plots, Porod's law, and Kratke-Porod's formula, can be calculated from the derivatives of  $\gamma(r)$  with different corresponding order to extract the various structural characteristics such as particle stiffness, global size, and interfacial inhomogeneities from small angle scattering spectra.<sup>69-72</sup> In Figure 4, we present the evolution of  $\gamma(r)$  calculated from the equilibrium MD trajectory with the inclusion of the effect of confined water structuring and intra-molecular voids (red curves). Due to the discrete nature of an atomistically simulated PAMAM dendrimer, the MD-generated  $\gamma(r)$  assumes the same role as pair distance distribution function  $p(r)$  which is the second moment of  $\gamma(r)$  (namely,  $r^2\gamma(r)$ ) in the continuum limit. This validity of argument can be demonstrated by the following mathematical derivations:

Before angular average  $\gamma(\vec{r})$  can be defined as

$$\begin{aligned}\gamma(\vec{r}) &= \frac{1}{nf_\gamma} \sum_i \sum_j \Delta\rho(\vec{r}_i) \Delta\rho(\vec{r}_j) \delta(\vec{r} - \vec{r}_i + \vec{r}_j) \\ &= \frac{1}{nf_\gamma} \sum_\Gamma \gamma(\vec{r}_\Gamma) \delta(\vec{r} - \vec{r}_\Gamma), \\ \vec{r}_\Gamma &= \vec{r}_i - \vec{r}_j.\end{aligned}\quad (8)$$

In Eq. (8),  $\Gamma$  indicates the summation is carried out over correlations between any two atoms in whole scattering contribu-

tors including polymeric components of dendrimers, confined water molecules, and counterions.  $nf_\gamma$  is a normalization factor.  $P(\vec{Q})$  can be obtained from following equation:

$$P(\vec{Q}) = \frac{1}{nf_\gamma} \int \gamma(\vec{r}) e^{-i\vec{Q}\cdot\vec{r}} d\vec{r} = \frac{1}{nf_\gamma} \sum_\Gamma \gamma(\vec{r}_\Gamma) e^{-i\vec{Q}\cdot\vec{r}_\Gamma}. \quad (9)$$

If  $\gamma(r)$  is continuous,  $P(\vec{Q})$  takes the following expression:

$$\begin{aligned}P(\vec{Q}) &= \frac{1}{nf_\gamma} \int \gamma(\vec{r}) e^{-i\vec{Q}\cdot\vec{r}} d\vec{r} \\ &= \frac{1}{nf_\gamma} \iiint \gamma(\vec{r}) e^{-i\vec{Q}\cdot\vec{r}} r^2 \sin(\theta) dr d\theta d\varphi \\ &= \frac{1}{nf_\gamma} \iiint p(\vec{r}) e^{-i\vec{Q}\cdot\vec{r}} \sin(\theta) dr d\theta d\varphi.\end{aligned}\quad (10)$$

From the last equalities on the RHS of Eqs. (9) and (10), the equivalence of  $\gamma(r)$  for a spatially discrete system and  $p(r)$  for the same system in continuous limit is clearly seen after the scalarizing process of Eq. (6). Evidenced by the documented scattering studies,<sup>28,29</sup>  $p(r)$  has been commonly used in various inverse scattering analyses for small angle scattering data analysis to find the size, shape, and internal structure of a scatterer from its measured scattering intensities.<sup>70,73-75</sup> The  $p(r)$  obtained from inverse Fourier transform of an experimentally determined  $P(Q)$  (black curves) is plotted in Figure 4 for comparison. Similar to the  $P(Q)$  presented in Figure 3, better agreement is seen between the MD and experimental  $p(r)$  for protonated dendrimer. In addition to the aforementioned orientational coupling issue which becomes more significant in the case of a neutral dendrimer due to its higher conformational aspect ratio, the quantitative accuracy of converting experimental  $P(Q)$  to  $p(r)$  is also hindered by the intrinsic limit embedded in the finite accessible  $Q$  range in a practical small angle scattering measurement. Unrealistic features could be introduced to  $p(r)$  via the necessary artificial smoothing and termination procedures for data transformation in this inverse approach. In this regard, providing sufficiently precise force field and proper trajectory analysis are adopted in simulation, the MD-generated  $p(r)$ , which is free from the constraint of limited spatial accessibility, is therefore mathematically advantageous to serve as a fundamental function to provide unbiased microscopic structural interpretation which is difficult to obtain experimentally. For example, with the availability of  $\gamma(r)$ , the structural implication of the bump



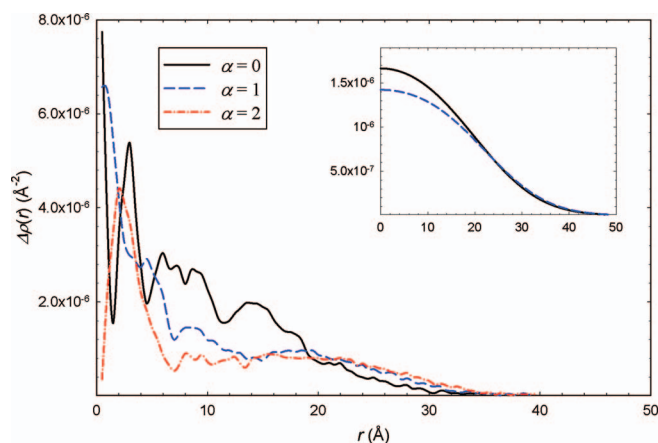


FIG. 5. The excess neutron scattering length density profiles  $\Delta\rho(r)$  of G4 PAMAM dendrimers obtained from MD simulation as a function of molecular protonation. The experimental  $\Delta\rho(r)$  (Ref. 35) determined from contrast variation SANS study is given in the inset.

centering around  $Q = 0.2 \text{ \AA}^{-1}$  in  $P(Q)$  for charged dendrimer shown in Figure 3 can be understood: The MD-generated  $p(r)$  presented in Figure 4 (red curves) becomes less skew around its peak and more unimodally distributed with the increase in molecular charge. Since  $p(r)$  gives the probability of finding atomic chords with a mutual distance between  $r$  and  $r + dr$  in the interior of dendrimer, the evolution of  $p(r)$  suggests the uniformization of the intra-dendrimer excess SLD distribution due to molecular charge and sphericalization of the dendrimer global shape. The bump in  $P(Q)$  can be viewed as a collective manifestation of these two factors.

Finally, we compare the MD-calculated structural characteristics of a G4 PAMAM dendrimer with our previous results obtained from contrast variation SANS experiments.<sup>38</sup> The angularly averaged excess neutron SLD profiles,  $\Delta\rho(r)$ , are given in Figure 5. Consistent with the evolution of  $\gamma(r)$  displayed in Figure 4, a charge-triggered outward SLD redistribution is seen. A similar trend is also observed in the evolution of the radial SLD distributions of polymeric components of dendrimer  $\rho(r)$  presented in Figure 6. As indicated by many previous simulation studies, under the charged

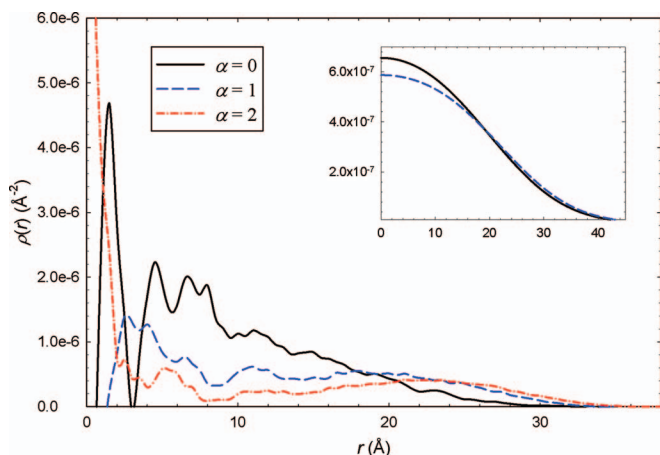


FIG. 6. The radial SLD distributions of polymer  $\rho(r)$  of G4 PAMAM dendrimers obtained from MD simulation at three different levels of molecular protonation. The experimental  $\rho(r)$  is given in the inset.

conditions, the entropy-driven backfolding process of the end groups is no longer energetically favorable due to an additional intra-molecular Coulomb repulsion. It is the outward relocation of these end groups which smears out the dense-core picture from the neutral dendrimer and renders a more uniformly distributed density profile at the charged state. However, whether this conformational change can be defined as a dense-core to dense-shell transition, as asserted by Goddard and coworkers<sup>16</sup> in their simulation study, remains subject of scientific debate. It is understood that the lack of dense-shell picture in  $\Delta\rho(r)$  and  $\rho(r)$  of charged dendrimer shown in the insets, which quantitatively agrees with MD-generated counterparts beyond the core region, is due to the form factor model based on Gaussian approximation of density profile. However, from the perspective of neutron scattering, due to the presence of the non-labile protons in the EDA core of PAMAM dendrimer, both  $\Delta\rho(r)$  and  $\rho(r)$  exhibit their highest values in the molecular core region, regardless the degree of molecular protonation. It is worth mentioning that a similar observation is also reported in Ref. 16. Second, the generally accepted dense-core picture of neutral dendrimer is reflected in the MD-generated  $p(r)$  with positive skewness (Figure 4(a)). The unskew unimodal distributions of  $p(r)$  for  $\alpha = 1$  (Figure 4(b)) and  $\alpha = 2$  (Figure 4(b)) clearly support the profile of a nearly uniform SLD distribution, instead of the dense-shell picture featured by a  $p(r)$  with negative skewness.

As demonstrated in our previous experimental study, the degree of molecular hydration, which is quantified by the number density of penetrating water molecules per unit volume  $H(r)$ , can be deduced from SANS fitting based on our developed model with two assumptions of negligible isotopic effect and geometric centrosymmetry of dendrimer.<sup>38</sup> The computational  $H(r)$  presented in Figure 7 is seen to increase in the core region of 15 Å and decrease in the corona region due to the outstretching end groups, which is qualitatively consistent with the evolution of  $\Delta\rho(r)$  and  $\rho(r)$  shown in Figures 5 and 6, respectively. Moreover, in comparison to the experimental results presented in the inset, the computed  $H(r)$  also shows considerable quantitative success in the

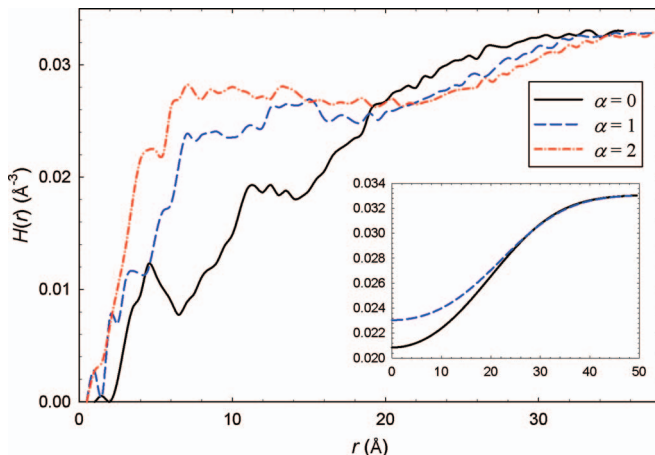


FIG. 7. The angularly averaged number density of invasive water per unit volume  $H(r)$  obtained MD simulation as a function of molecular protonation. The experimentally determined  $H(r)$  is given in the inset.



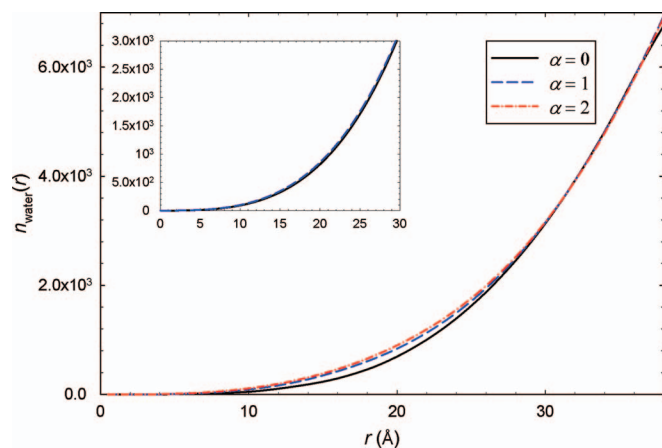


FIG. 8. The total number of invasive water  $n_{\text{water}}(r)$  obtained from MD simulation as a function of molecular protonation. The SANS determined values are presented in the inset.

prediction of the evolution of intra-molecular hydration as a function of molecular protonation, especially in the spatial region ranging from 10 Å to the molecular periphery along the radial direction of dendrimer.

Figure 8 gives the total invasive water population along the radial direction  $n_{\text{water}}(r)$ , which is obtained from evaluating the spatial integral with the MD-predicted  $H(r)$  as the integrand. A generally good quantitative agreement between the MD predictions and the experimental results obtained from contrast variation SANS investigation is seen for dendrimer with different degree of molecular protonation. Nevertheless, a minor increase in  $n_{\text{water}}(r)$  within the intra-molecular region from 10 Å to 30 Å is predicted but was not observed by contrast variation SANS investigation within experimental uncertainties, probably due to the limitation of instrumental resolution and various aforementioned constraints of the theoretical model of coherent scattering cross section for PAMAM dendrimer used in SANS data analysis.

#### IV. CONCLUSIONS

In this report, the SANS intensity behavior of G4 PAMAM dendrimer is investigated using atomistic MD simulation at different levels of molecular protonation. Two different correlation functions, the small angle neutron scattering form factor  $P(Q)$  and the Debye correlation function  $\gamma(r)$ , are calculated from the equilibrium trajectories based on a methodology which rigorously incorporates the scattering contributions from the compositional and density fluctuations of the dendrimer, the counterions, and the water. The critical influence of confined water on the microstructure of a dendrimer dissolved in water is evidenced by the necessity of including the additional scattering signature contributed by the interfacial and intra-molecular water density fluctuation in the MD-predicted  $P(Q)$  for improved agreement with experiment. The validity of this proposed trajectory analysis approach is further demonstrated by the satisfactory quantitative agreement between computational prediction and experiment on several computationally structural characteristics such as excess and polymeric scattering length

density profiles and degree of hydration. This methodology developed in this work could also be applied to bridge the link between computational and experimental scattering functions for the general colloidal systems in which confined water structuring is relevant to their microstructure, such as protein solutions, to investigate the effect of interfacial water structuring, and therefore it could benefit other researchers in the larger field of soft matter.

#### ACKNOWLEDGMENTS

This Research at Oak Ridge National Laboratory's Spallation Neutron Source was sponsored by the Scientific User Facilities Division, Office of Basic Energy Sciences, U.S. Department of Energy. We thank the ORNL Institutional Cluster (OIC) for the computational support.

- <sup>1</sup>M. Ballauff and C. N. Likos, *Angew. Chem., Int. Ed.* **43**, 2998 (2004).
- <sup>2</sup>C. N. Likos, *Soft Matter* **2**, 478 (2006).
- <sup>3</sup>C. C. Lee, J. A. MacKay, J. M. J. Fréchet, and F. C. Szoka, *Nat. Biotechnol.* **23**, 1517 (2005).
- <sup>4</sup>D. Astruc, E. Boisselier, and C. Omelas, *Chem. Rev.* **110**, 1857 (2010).
- <sup>5</sup>P. Welch and M. Muthukumar, *Macromolecules* **31**, 5892 (1998).
- <sup>6</sup>I. Lee, B. D. Athey, A. W. Wetzel, W. Meixner, and J. R. Baker, *Macromolecules* **35**, 4510 (2002).
- <sup>7</sup>P. K. Maiti, T. Çağun, S.-T. Lin, and W. A. Goddard, *Macromolecules* **38**, 979 (2005).
- <sup>8</sup>H. Lee, J. R. Baker, and Ronald G. Larson, *J. Phys. Chem. B* **110**, 4014 (2006).
- <sup>9</sup>P. K. Maiti and W. A. Goddard, *J. Phys. Chem. B* **110**, 25628 (2006).
- <sup>10</sup>A. W. Opitz and N. J. Wagner, *J. Polym. Sci., Part B: Polym. Phys.* **44**, 3062 (2006).
- <sup>11</sup>G. Giupponi, D. M. A. Buzza, and D. Adolf, *Macromolecules* **40**, 5959 (2007).
- <sup>12</sup>K. Karatasos, *Macromolecules* **41**, 1025 (2008).
- <sup>13</sup>R. Blaak, S. Lehmann, and C. N. Likos, *Macromolecules* **41**, 4452 (2008).
- <sup>14</sup>J. J. Freire, *Soft Matter* **4**, 2139 (2008).
- <sup>15</sup>J. S. Kłos and J.-U. Sommer, *Macromolecules* **42**, 4878 (2009).
- <sup>16</sup>Y. Liu, V. S. Bryantsev, M. S. Diallo, and W. A. Goddard, *J. Am. Chem. Soc.* **131**, 2798 (2009).
- <sup>17</sup>I. Tanis and K. Karatasos, *J. Phys. Chem. B* **113**, 10984 (2009).
- <sup>18</sup>W. Tian and Y. Ma, *J. Phys. Chem. B* **113**, 13161 (2009).
- <sup>19</sup>S. Huißmann, A. Wynveen, C. N. Likos, and R. Blaak, *J. Phys.: Condens. Matter* **22**, 232101 (2010).
- <sup>20</sup>S. Huißmann, C. N. Likos, and R. Blaak, *J. Mater. Chem.* **20**, 10486 (2010).
- <sup>21</sup>W. Tian and Y. Ma, *Soft Matter* **6**, 1308 (2010).
- <sup>22</sup>J. S. Kłos and J.-U. Sommer, *Macromolecules* **43**, 4418 (2010).
- <sup>23</sup>J. S. Kłos and J.-U. Sommer, *Macromolecules* **43**, 10659 (2010).
- <sup>24</sup>H. Lee and Ronald G. Larson, *Macromolecules* **44**, 2291 (2011).
- <sup>25</sup>K. Karatasos and I. Tanis, *Macromolecules* **44**, 6605 (2011).
- <sup>26</sup>S. Huißmann, C. N. Likos, and R. Blaak, *Soft Matter* **7**, 8149 (2011).
- <sup>27</sup>S.-H. Chen, *Annu. Rev. Phys. Chem.* **37**, 351 (1986).
- <sup>28</sup>*Neutron, X-rays and Light: Scattering: Introduction to an Investigation Tool for Colloidal and Polymeric Systems*, edited by P. Linder and Th. Zemb (North-Holland, Amsterdam, 1991).
- <sup>29</sup>*Neutron, X-rays and Light: Scattering Methods Applied to Soft Condensed Matter*, edited by P. Linder and Th. Zemb (North-Holland, Amsterdam, 2002).
- <sup>30</sup>W.-R. Chen, L. Porcar, Y. Liu, P. D. Butler, and L. J. Magid, *Macromolecules* **40**, 5887 (2007).
- <sup>31</sup>L. Porcar, Y. Liu, R. Verduzco, K. Hong, P. D. Butler, L. J. Magid, G. S. Smith, and W.-R. Chen, *J. Phys. Chem. B* **112**, 14772 (2008).
- <sup>32</sup>T. Li, L. Porcar, Y. Liu, P. D. Butler, and W.-R. Chen, *Macromolecules* **41**, 8916 (2008).
- <sup>33</sup>L. Porcar, K. Hong, P. D. Butler, K. W. Herwig, G. S. Smith, Y. Liu, and W.-R. Chen, *J. Phys. Chem. B* **114**, 1751 (2010).
- <sup>34</sup>Y. Liu, L. Porcar, K. Hong, C.-Y. Shew, X. Li, E. Liu, P. D. Butler, K. W. Herwig, G. S. Smith, and W.-R. Chen, *J. Chem. Phys.* **132**, 124901 (2010).

- <sup>35</sup>Y. Liu, C.-Y. Chen, H.-L. Chen, K. Hong, C.-Y. Shew, X. Li, E. Liu, P. D. Butler, K. W. Herwig, G. S. Smith, L. Porcar, and W.-R. Chen, *J. Phys. Chem. Lett.* **1**, 2020 (2010).
- <sup>36</sup>X. Li, M. Zamponi, K. Hong, L. Porcar, C.-Y. Shew, T. Jenkins, E. Liu, G. S. Smith, K. W. Herwig, Y. Liu, and W.-R. Chen, *Soft Matter* **7**, 618 (2011).
- <sup>37</sup>K. Hong, Y. Liu, L. Porcar, D. Liu, C. Y. Gao, G. S. Smith, K. W. Herwig, S. Cai, X. Li, B. Wu, W.-R. Chen, and E. L. Liu, *J. Phys.: Condens. Matter* **24**, 064116 (2012).
- <sup>38</sup>B. Wu, X. Li, C. Do, T.-W. Kim, Y. Liu, J. Yang, K. Hong, L. Porcar, C.-Y. Shew, E. L. Liu, G. S. Smith, K. W. Herwig, and W.-R. Chen, *J. Chem. Phys.* **135**, 144903 (2011).
- <sup>39</sup>S. V. Lyulin, A. A. Darinskii, A. V. Lyulin, and M. A. J. Michels, *Macromolecules* **37**, 4676 (2004).
- <sup>40</sup>In their own activities as scientific institutions, NIST and ORNL use many different materials, products, types of equipment, and services. However, NIST and ORNL do not approve, recommend, or endorse any product or proprietary material.
- <sup>41</sup>P. K. Maiti and B. Bagchi, *Nano Lett.* **6**, 2478 (2006).
- <sup>42</sup>C. Jana, G. Jayamurugan, R. Ganapathy, P. K. Maiti, N. Jayaraman, and A. K. Sood, *J. Chem. Phys.* **124**, 240719 (2006).
- <sup>43</sup>P. K. Maiti and B. Bagchi, *J. Chem. Phys.* **131**, 214901 (2009).
- <sup>44</sup>J. Wang, W. Wang, P. A. Kollman, and D. A. Case, *J. Mol. Graphics Modell.* **25**, 247 (2006).
- <sup>45</sup>J. Wang, R. M. Wolf, J. W. Caldwell, P. A. Kollman, and D. A. Case, *J. Comput. Chem.* **25**, 1157 (2004).
- <sup>46</sup>D. A. Case, T. A. Darden, T. E. Cheatham III, C. L. Simmerling, J. Wang, R. E. Duke, R. Luo, R. C. Walker, W. Zhang, K. M. Merz, B. P. Roberts, B. Wang, S. Hayik, A. Roitberg, G. Seabra, I. Kolossvai, K. F. Wong, F. Paesani, J. Vanicek, J. Liu, X. Wu, S. R. Brozell, T. Steinbrecher, H. Gohlke, Q. Cai, X. Ye, J. Wang, M.-J. Hsieh, G. Cui, D. R. Roe, D. H. Mathews, M. G. Seetin, C. Sagui, V. Babin, T. Luchko, S. Gusarov, A. Kovalenko, and P. A. Kollman, AMBER 11, University of California, San Francisco, 2010.
- <sup>47</sup>W. L. Jorgensen, *J. Am. Chem. Soc.* **103**, 335 (1981).
- <sup>48</sup>R. W. Pastor, B. R. Brooks, and A. Szabo, *Mol. Phys.* **65**, 1409 (1988).
- <sup>49</sup>U. L. Essmann, L. Perera, M. L. Berkowitz, T. Darden, H. Lee, and L. G. Pedersen, *J. Chem. Phys.* **103**, 8577 (1995).
- <sup>50</sup>J. P. Ryckaert, G. Ciccotti, and H. J. C. Berendsen, *J. Comput. Phys.* **23**, 327 (1977).
- <sup>51</sup>O. Spalla, in *Neutron, X-rays and Light: Scattering Methods Applied to Soft Condensed Matter*, edited by P. Linder and Th. Zemb (North-Holland, Amsterdam, 2002), pp. 49–71.
- <sup>52</sup>L. Belloni, *J. Phys.: Condens. Matter* **12**, R549 (2000).
- <sup>53</sup>R. G. Horn and B. W. Ninham, in *Micellar Solutions and Microemulsions: Structure, Dynamics, and Statistical Thermodynamics*, edited by S.-H. Chen and R. Rajagopalan (Springer-Verlag, New York, 1990), pp. 81–97.
- <sup>54</sup>J. Israelachvili, *Intermolecular & Surface Forces*, 2nd ed. (Academic Press, Amsterdam, 1992).
- <sup>55</sup>J. W. Verwey and J. Th. G. Overbeek, *Theory of the Stability of Lyophobic Colloids* (Elsevier, Amsterdam, 1948).
- <sup>56</sup>C. Rau and V. A. Parsegian, *Science* **249**, 1278 (1990).
- <sup>57</sup>C. Rau and V. A. Parsegian, *Biophys. J.* **61**, 260 (1992).
- <sup>58</sup>N. Petsev and P. G. Vekilov, *Phys. Rev. Lett.* **84**, 1339 (2000).
- <sup>59</sup>T. Suzuki, H. Endo, and M. Shibayama, *Langmuir* **24**, 4537 (2008).
- <sup>60</sup>E. Mamontov, L. Vlcek, D. J. Wesolowski, P. T. Cummings, W. Wang, L. M. Anovitz, J. Rosenqvist, C. M. Brown, and V. Garcia Sakai, *J. Phys. Chem. C* **111**, 4328 (2007).
- <sup>61</sup>J.-P. Hansen and I. R. McDonald, *Theory of Simple Liquids*, 3rd ed. (Elsevier, Amsterdam, 2006).
- <sup>62</sup>T. Egami and S. J. L. Billinge, *Underneath the Bragg Peaks: Structural Analysis of Complex Materials* (Pergamon, Amsterdam, 2003).
- <sup>63</sup>W. Humphrey, A. Dalke, and K. Schulten, *J. Mol. Graphics* **14**, 33 (1996).
- <sup>64</sup>P. Debye and A. M. Bueche, *J. Appl. Phys.* **20**, 518 (1949).
- <sup>65</sup>O. Glatter, *Acta Phys. Austriaca* **47**, 83 (1977).
- <sup>66</sup>A. Guinier, G. Fournet, C. B. Walker, and K. L. Yudowitch, *Small-Angle Scattering of X-Rays* (Wiley, New York, 1955).
- <sup>67</sup>For example, see D. J. Price and C. L. Brooks, *J. Chem. Phys.* **121**, 10096 (2004).
- <sup>68</sup>R. Kubo, *Statistical Mechanics* (North-Holland, Amsterdam, 1965).
- <sup>69</sup>*Small Angle X-ray Scattering*, edited by O. Glatter and O. Kratky (Academic, London, 1982).
- <sup>70</sup>L. Feigin and D. L. Svergun, *Structure Analysis by Small-Angle X-Ray and Neutron Scattering* (Plenum, New York, 1987).
- <sup>71</sup>S. Ciccariello, *J. Math. Phys.* **36**, 219 (1995).
- <sup>72</sup>W. Gille, *Eur. Phys. J. B* **17**, 371 (2000).
- <sup>73</sup>O. Glatter, in *Small Angle X-ray Scattering*, edited by O. Glatter and O. Kratky (Academic, London, 1982), pp. 167–196.
- <sup>74</sup>O. Glatter, in *Neutron, X-rays and Light: Scattering: Introduction to an Investigation Tool for Colloidal and Polymeric Systems*, edited by P. Linder and Th. Zemb (North-Holland, Amsterdam, 1991), pp. 33–82.
- <sup>75</sup>O. Glatter, in *Neutron, X-rays and Light: Scattering Methods Applied to Soft Condensed Matter*, edited by P. Linder and Th. Zemb (North-Holland, Amsterdam, 2002), pp. 73–102.